Neuron, Vol. 42, 101–112, April 8, 2004, Copyright ©2004 by Cell Press

A Voltage-Gated Calcium-Selective Channel Encoded by a Sodium Channel-like Gene

Wei Zhou,[1,3] Inbum Chung,[2,3] Zhiqi Liu,[2] Alan L. Goldin,[1,*] and Ke Dong[2,*]
[1]Department of Microbiology and Molecular Genetics
University of California, Irvine
Irvine, California 92697
[2]Department of Entomology and
Neuroscience Program
Michigan State University
East Lansing, Michigan 48824

Summary

BSC1, which was originally identified by its sequence similarity to voltage-gated Na^+ channels, encodes a functional voltage-gated cation channel whose properties differ significantly from Na^+ channels. BSC1 has slower kinetics of activation and inactivation than Na^+ channels, it is more selective for Ba^{2+} than for Na^+, it is blocked by Cd^{2+}, and Na^+ currents through BSC1 are blocked by low concentrations of Ca^{2+}. All of these properties are more similar to voltage-gated Ca^{2+} channels than to voltage-gated Na^+ channels. The selectivity for Ba^{2+} is partially due to the presence of a glutamate in the pore-forming region of domain III, since replacing that residue with lysine (normally present in voltage-gated Na^+ channels) makes the channel more selective for Na^+. BSC1 appears to be the prototype of a novel family of invertebrate voltage-dependent cation channels with a close structural and evolutionary relationship to voltage-gated Na^+ and Ca^{2+} channels.

Introduction

Voltage-gated Na^+ channels are responsible for the rising phase of the action potential in the membranes of neurons and most electrically excitable cells (Catterall, 2000). They are members of a superfamily that also includes voltage-gated K^+ channels, voltage-gated Ca^{2+} channels, and cyclic nucleotide-gated channels (Hille, 2001; Jan and Jan, 1992). The Na^+ and Ca^{2+} channels contain four homologous domains, whereas the K^+ and cyclic nucleotide-gated channels consist of tetramers of single-domain subunits. It is generally believed that Na^+ and Ca^{2+} channels evolved from the single-domain K^+ channels (Hille, 1987, 1988). The proposed scenario is that Ca^{2+} channels evolved from the K^+ channels during the evolution of the stem eukaryotes (Hille, 1989). Because no K^+ channels with multiple homologous domains have been observed, it is assumed that the selectivity change from K^+ to Ca^{2+} occurred before the gene duplication event (Anderson and Greenberg, 2001). Na^+ channels then evolved from an ancestral channel resembling the T type (Ca_v3 family) Ca^{2+} channels (Spafford et al., 1999). Consistent with this hypothesis, the four domains of the Na^+ channel are more similar to the four domains of the Ca^{2+} channels than to each other (Hille, 1989; Strong et al., 1993). This hypothesis predicts the existence of an ancestral four-domain channel with properties intermediate between Ca^{2+} and Na^+ channels. A descendant of such a channel might be one of the four-domain proteins that are homologous to Na^+ and Ca^{2+} channels but have not been functionally expressed.

More than 50 genes encoding Na^+ channels have been cloned from animals, including at least 18 from invertebrate species, most of which have not been functionally expressed (Goldin, 2002). The invertebrate Na^+ channel genes include two Na^+ channel-like genes from insects, *DSC1* and *para*. *DSC1* was originally isolated from a *Drosophila* genomic DNA library using an eel Na^+ channel cDNA probe (Salkoff et al., 1987), and *para* was identified using temperature-sensitive paralysis phenotypes displayed by mutant alleles in *Drosophila* (Loughney et al., 1989). Orthologous genes (*BSC1* and *para*^{CSMA}) from German cockroach (*Blattella germanica*) have since been identified (Dong, 1997; Liu et al., 2001). The deduced amino acid sequences and the overall domain organization of these genes are very similar to those of known voltage-gated Na^+ channels. However, only *para* (from *Drosophila*, cockroach, and house fly) has been functionally expressed and shown to encode a voltage-gated Na^+ channel (Feng et al., 1995; Smith et al., 1997; Tan et al., 2002a, 2002b; Warmke et al., 1997). One possible explanation for the lack of DSC1 or BSC1 function is that these proteins require unique auxiliary subunits for efficient expression, as is the case for *Drosophila para* (Feng et al., 1995; Warmke et al., 1997). However, an alternative explanation is that *DSC1* and *BSC1* encode channels with different functional properties compared to Na^+ channels so that the recording conditions that were utilized were not appropriate for these channels.

In this study, we successfully expressed BSC1 channels in *Xenopus* oocytes and demonstrated that *BSC1* encodes a voltage-gated Ca^{2+}-selective channel that is intermediate between voltage-gated Na^+ and Ca^{2+} channels. These data suggest that BSC1 is the prototype of a novel family of invertebrate voltage-dependent cation channels with a close structural and evolutionary relationship to voltage-gated Na^+ and Ca^{2+} channels.

Results

BSC1 Currents in *Xenopus* Oocytes

The deduced amino acid similarity of BSC1 with known voltage-gated Na^+ channel proteins was 30%–35% overall and 45%–50% in the four homologous domains (Liu et al., 2001). Therefore, we initially hypothesized that the *BSC1* gene encodes a Na^+ channel. However, we did not detect any Na^+ current in *Xenopus* oocytes expressing BSC1 during 10 ms depolarizations to test potentials between −50 and 100 mV from a holding potential of −100 mV in ND96 using a two-electrode

*Correspondence: dongk@msu.edu (K.D.); agoldin@uci.edu (A.L.G.)
[3]These authors contributed equally to this work.

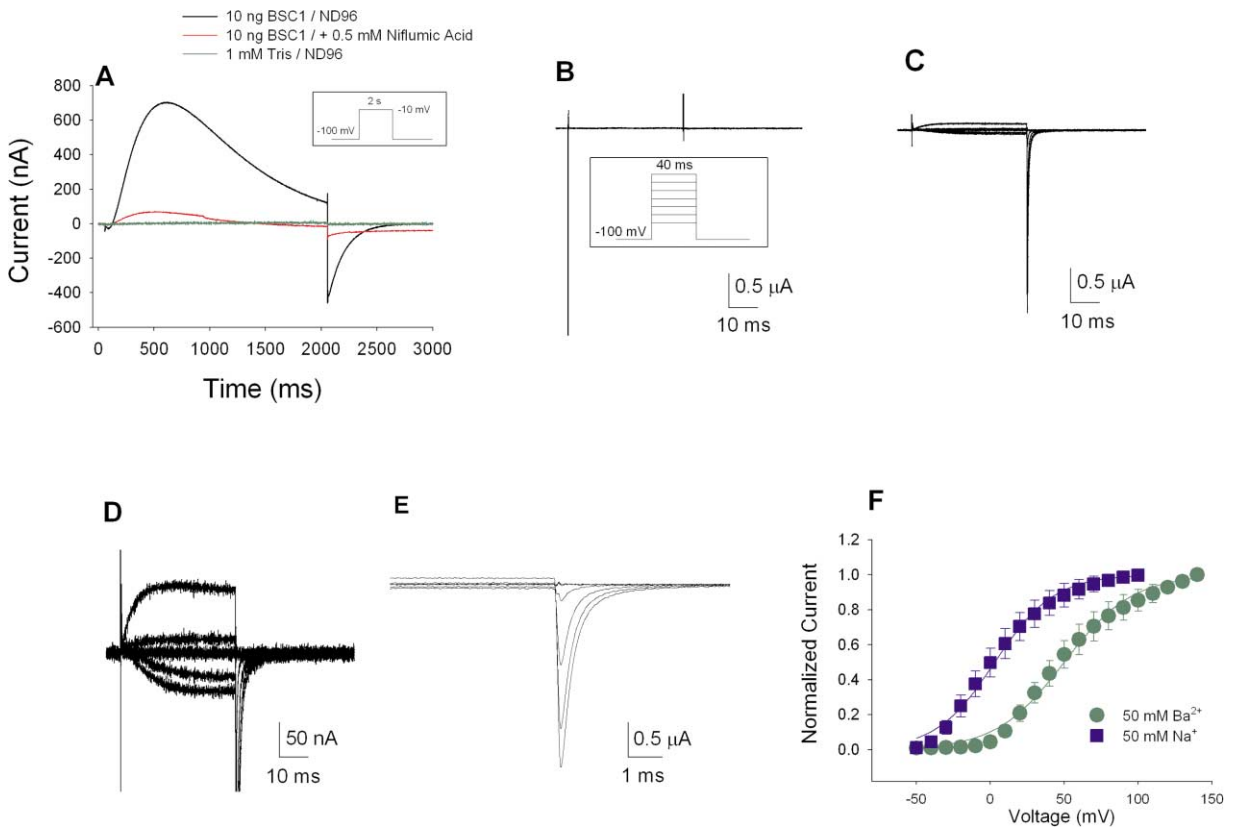

Figure 1. Characterization of the BSC1 Channel in *Xenopus* Oocytes

(A) Injection of 10 ng BSC1 RNA resulted in a significant outward current in oocytes 4 days after injection (black). The protocol consisted of a 2 s depolarization from −100 to −10 mV followed by repolarization to −100 mV (inset). The external solution consisted of ND96. Replacing the external solution with ND96 plus 0.5 mM niflumic acid, a Cl^- channel blocker, eliminated most of the outward current (red). The outward current was not present in oocytes injected with 1 mM Tris (green).

(B) No current was observed in oocytes injected with 1 mM Tris. The protocol consisted of 40 ms depolarizations from −100 mV to potentials ranging from −50 to 140 mV in 10 mV increments followed by repolarization to −100 mV (inset). Every other current trace from −50 to 70 mV is shown. The external solution consisted of 50 mM $Ba(OH)_2$, 55 mM TEAOH, and 5 mM HEPES.

(C) Current in an oocyte injected with 5 ng BSC1 RNA using the same protocol and recording conditions as in (B).

(D) The currents from (C) are shown on an expanded current scale.

(E) The tail currents from (C) are shown on an expanded time scale.

(F) The voltage dependence of activation was determined by measuring the tail currents in experiments similar to the ones shown in (C) and (E), followed by normalization to the maximum tail current. The normalized values were plotted against the voltage of depolarization, and the data were fit with a two-state Boltzmann equation as described in Experimental Procedures. The external solution consisted of either 50 mM $Ba(OH)_2$, 55 mM TEAOH, and 5 mM HEPES (green circles) or 50 mM NaOH, 45 mM TEAOH, 10 mM HEPES, and 10 mM HEDTA (blue squares). The parameters of the fits are an apparent gating charge of 1.1 ± 0.2 and a half-maximal activation voltage of 50 ± 8 mV in 50 mM Ba^{2+} and an apparent gating charge of 1.3 ± 0.3 and a half-maximal activation voltage of 3 ± 7 mV in 50 mM Na^+.

voltage clamp. Similar recording conditions routinely elicit robust Na^+ currents in oocytes expressing cockroach $Para^{CSMA}$ (Tan et al., 2002b). When the duration of the depolarization pulses was increased to 2 s, however, a slow outward current was observed (Figure 1A, black). No significant outward current was observed in Tris-injected oocytes (Figure 1A, green). The slow outward current was greatly reduced by including 0.5 mM niflumic acid in the recording solution (Figure 1A, red). Since niflumic acid is a Cl^- channel blocker, these results suggest that the outward current represents a Ca^{2+}-activated Cl^- current. Consistent with this interpretation, the slow outward current was not observed in oocytes injected with 45 nl of 50 mM BAPTA (1,2-bis[2-aminophenoxy]-ethane-N, N, N′, N′-tetraacetic acid), a Ca^{2+} chelator (data not shown). Based on these results, we speculated that the BSC1 channel was permeable to Ca^{2+} and that Ca^{2+} influx through the BSC1 channels activated endogenous Ca^{2+}-activated Cl^- channels, which are known to be present in *Xenopus* oocytes (Kuruma and Hartzell, 2002).

Since BSC1 appeared to function as a voltage-gated cation channel, we recorded currents through BSC1 channels using conditions appropriate for voltage-gated Ca^{2+} channels. The external solution contained 50 mM Ba^{2+} as a charge carrier instead of Ca^{2+} to prevent the activation of endogenous Ca^{2+}-activated Cl^- channels, and Cl^- was not included in the recording solution. In addition, 55 mM tetraethylammonium (TEA^+) was included in the recording solution to inhibit endogenous voltage-gated K^+ channels. With capacity and resistance compensation and P/4 subtraction, the capacity transient was compensated within 0.1 ms of the voltage command change so that we could accurately measure

peak currents. We first examined the voltage dependence of channel activation by depolarizing the membrane from a holding potential of −100 mV to a range of potentials between −50 mV and 140 mV for 40 ms, followed by repolarization to −100 mV. As shown in Figure 1B, Tris-injected oocytes demonstrated no significant current under these conditions. In contrast, oocytes injected with BSC1 RNA showed slowly activating, voltage-dependent currents during the depolarization (Figures 1C and 1D). The 40 ms depolarization was long enough to fully activate the channels, since the current reached a maximum amplitude and stabilized within this time period. There was no apparent inactivation within 40 ms. Upon repolarization, large inward tail currents that were most likely carried by Ba^{2+} were observed (Figures 1C and 1E).

The peak tail current after each depolarization was normalized to the maximum tail current after 140 mV and plotted against voltage (Figure 1F, green circles). The current does not appear to have reached a maximum by 140 mV, but we were unable to use higher depolarization voltages, because the tail currents were contaminated with outward Cl^{-} currents resulting from activation of endogenous Cl^{-} channels at voltages more positive than 140 mV. The contaminating Cl^{-} currents could be distinguished from the Ba^{2+} currents flowing through the BSC1 channels because of their slower kinetics, but they could not be eliminated or subtracted. The voltage dependence of BSC1 channel activation was fit to a two-state Boltzmann function as described in Experimental Procedures, resulting in an apparent gating charge of 1.1 ± 0.2 and a half-maximal activation voltage of 50 ± 8 mV.

Kinetics of Channel Activation and Inactivation

The kinetics of activation and inactivation appeared to be much slower for the BSC1 channels compared to typical voltage-gated Na^{+} channels, with no significant inactivation during a 40 ms depolarization. To more accurately examine the kinetics of activation and inactivation, we used a series of depolarizations from −100 mV to 80 mV followed by a return to −100 mV, with increasing depolarization times (Figure 2A). The amplitudes of the tail currents increased until about 30 ms, indicating increasing channel activation, after which the amplitudes slowly decreased due to inactivation of the channels.

The kinetics of activation were measured during depolarizations to 80 mV ranging from 1 ms to 30 ms. The tail current after each depolarization was normalized to the maximum tail current after a 30 ms depolarization and plotted against the time of depolarization (Figure 2B). The data were fit with a single exponential equation, resulting in a time constant for channel activation at 80 mV of 5.9 ± 0.8 ms. To measure inactivation, tail currents were measured after depolarizations to 80 mV for longer periods of time extending to 500 ms (Figure 2C). Inactivation was not complete during this time period, with approximately 40% of the current remaining at the end of a 500 ms depolarization. We were unable to record tail currents for depolarizations longer than 500 ms because of the endogenous Cl^{-} currents, which also resulted in the large standard deviations at the later time points. The inactivation process was fit with a single exponential equation, resulting in an inactivation time constant of 235 ± 21 ms with a steady-state asymptote of 40% ± 30%.

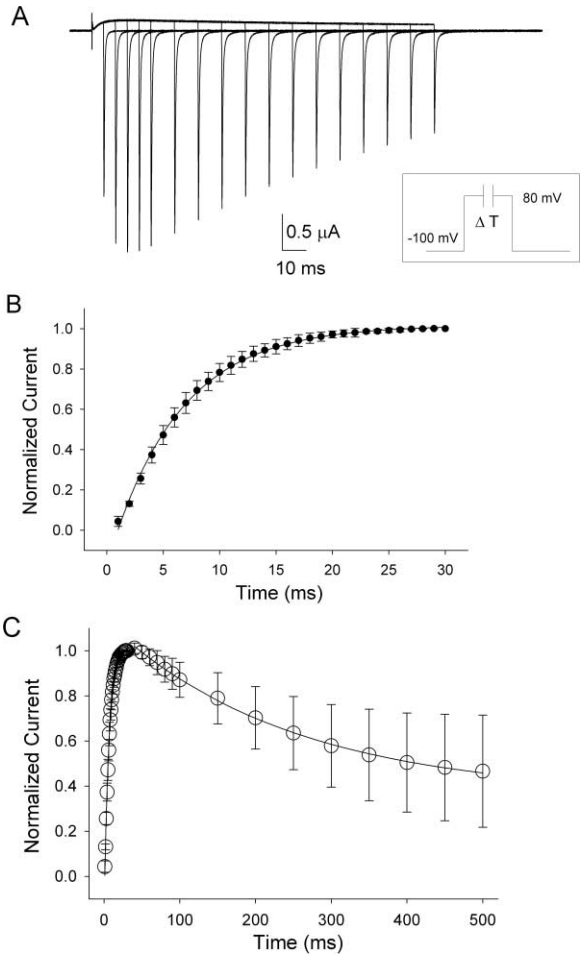

Figure 2. Kinetics of BSC1 Channel Gating

(A) The kinetics of BSC1 activation and inactivation were measured by a series of depolarizations from −100 to 80 mV for 5–150 ms in 5 ms increments, followed by repolarization to −100 mV. The protocol is shown in the inset. The oocytes were injected with 5 or 10 ng BSC1 RNA, and the external solution contained 50 mM $Ba(OH)_2$, 55 mM TEAOH, and 5 mM HEPES. Traces are shown from 5 to 25 ms in 5 ms increments and from 35 to 145 ms in 10 ms increments.

(B) The kinetics of activation were determined by depolarizations from 1 to 30 ms in 1 ms increments. The peak tail current following each depolarization was normalized to the maximal peak tail current and plotted against the time of depolarization. The smooth curve represents the best fit to a single exponential equation. The channels were fully activated after a 30 ms depolarization (τ = 5.9 ± 0.8 ms).

(C) The kinetics of inactivation were determined by longer depolarizations, up to 500 ms in 5 or 50 ms increments. The peak tail current following each depolarization was normalized to the maximal peak tail current and plotted against the time of depolarization. The smooth curve represents the best fit to a single exponential equation (τ = 235 ± 21 ms, steady-state asymptote = 40% ± 30%).

Selectivity of the BSC1 Channel

The kinetics of activation indicated that more than 90% of the current through BSC1 channels was activated after 20 ms at 80 mV (Figure 2). Given these results, it seemed surprising that we did not observe any current in ND96 after 20 ms at 50 mV. One explanation for the

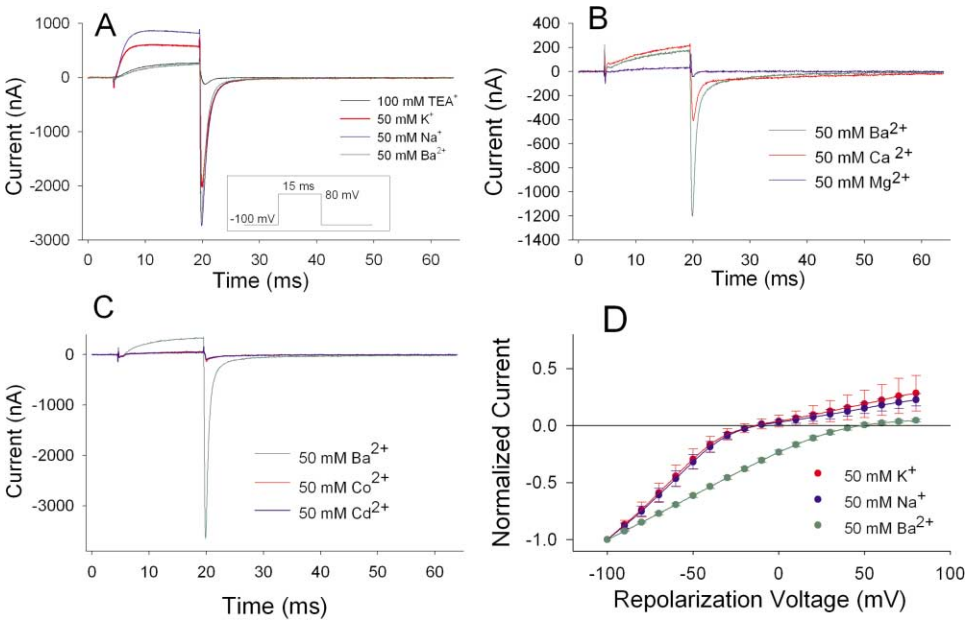

Figure 3. Ion Selectivity of the BSC1 Channel

(A) Currents were recorded from an oocyte injected with 5 ng BSC1 RNA using different external solutions as follows: 100 mM TEAOH + 10 mM HEPES (black), 50 mM KOH + 45 mM TEAOH + 10 mM HEPES + 10 mM HEDTA (red), 50 mM NaOH + 45 mM TEAOH + 10 mM HEPES + 10 mM HEDTA (blue), or 50 mM $Ba(OH)_2$ + 55 mM TEAOH + 5 mM HEPES (green). The protocol consisted of a depolarization from −100 mV to 80 mV for 15 ms followed by repolarization to −100 mV (inset).

(B) Currents were recorded from an oocyte injected with 5 ng BSC1 RNA using different external solutions as follows: 50 mM $Ba(OH)_2$ + 55 mM TEAOH + 5 mM HEPES (green), 50 mM $Ca(OH)_2$ + 55 mM TEAOH + 10 mM HEPES (red), or 50 mM $Mg(OH)_2$ + 55 mM TEAOH + 10 mM HEPES (blue).

(C) Currents were recorded from an oocyte injected with 5 ng BSC1 RNA using different external solutions as follows: 50 mM $Ba(OH)_2$ + 55 mM TEAOH + 5 mM HEPES (green), 50 mM $Co(OH)_2$ + 55 mM TEAOH + 10 mM HEPES (red), or 50 mM $Cd(OH)_2$ + 55 mM TEAOH + 10 mM HEPES (blue).

(D) Tail currents were measured by depolarization to 80 mV followed by repolarization to different potentials in each external solution, after which the tail currents were normalized to the peak tail current and plotted against the repolarization voltage. The recording solutions were as follows: 50 mM Ba^{2+} (green), 50 mM Na^+ (blue), or 50 mM K^+ (red).

lack of current is that the composition of the external ND96 solution may have prevented current flow through the BSC1 channels. For example, voltage-gated Ca^{2+} channels are highly selective for Ca^{2+} under normal conditions, in which selectivity against monovalent ions is achieved by binding of Ca^{2+} with micromolar affinity to the channel pore. Therefore, low concentrations of Ca^{2+} can prevent permeation by monovalent ions even if the concentration of Ca^{2+} is insufficient to conduct detectable current. ND96 contains a high concentration of Na^+ (96 mM), which should permeate through the BSC1 channels, but it also contains a significant concentration of Ca^{2+} (1.8 mM). The 1.8 mM Ca^{2+} in ND96 may have blocked permeation by monovalent ions so that no Na^+ currents were observed, but the Ca^{2+} concentration may not have been high enough to conduct detectable current.

If this hypothesis is correct, then it should be possible to observe BSC1 currents carried by monovalent cations in the absence of external Ca^{2+}. Figure 3A shows BSC1 currents recorded with equivalent concentrations of different monovalent cations in the external solutions, as listed in Table 1, section A. Currents were first recorded using an external solution containing only 100 mM TEA^+ as a control, because it was always necessary to include TEA^+ to block the endogenous voltage-gated K^+ channels. There was a small outward current during the depolarization to 80 mV and a negligible inward tail current when the oocyte was repolarized to −100 mV (black), indicating that the channel has very low permeability to TEA^+. When the external solution was replaced with 50 mM Ba^{2+} and 55 mM TEA^+ (green), the outward current was similar in magnitude to the current in TEA^+, but there was a large inward tail current, indicating that the BSC1 channels have a high permeability to divalent ions. When the external solution was replaced with 50 mM K^+ plus 45 mM TEA^+ and 10 mM HEDTA to chelate any residual Ca^{2+}, a large outward current was observed during the depolarization to 80 mV, and this was followed by a large tail current (red). The outward current was most likely due to K^+ ions that are no longer blocked by the free Ca^{2+} ions, and the inward current most likely resulted from an influx of K^+. Finally, when the external solution was replaced with 50 mM Na^+ plus 45 mM TEA^+ and 10 mM HEDTA, both the outward current during the depolarization and the tail current were larger than with K^+ outside (blue). The larger outward current is most likely due to the increased driving force resulting from the low external K^+ compared to the high internal K^+, and the inward current is most likely due to the high external Na^+.

To examine the relative permeability of different diva-

Table 1. Composition of External Solutions

A. External Solutions with Different Permeant Cations

Permeant Ion	Na^+	K^+	Ba^{2+}	Ca^{2+}	Mg^{2+}	Co^{2+}	Cd^{2+}	None	
Hydroxide (mM)	50	50	50	50	50	50	50	0	
HEPES (mM)	10	10	5	10	10	10	10	10	
HEDTA (mM)	10	10	0	0	0	0	0	0	
TEAOH (mM)	45	45	55	55	55	55	55	100	

B. External Solutions with Different Free Ca^{2+} Concentrations

Free [Ca^{2+}] (mM)	2×10^{-6}	2×10^{-5}	2×10^{-4}	0.002	0.02	0.2	2	10	20
$Ca(OH)_2$ (mM)	10	10	10	10	10	10	10	10	20
HEDTA (mM)	35	13	10	0	0	0	8	0	0
HIDA (mM)	0	0	0	15	11	10	0	0	0
TEAOH (mM)	35	57	60	55	59	60	62	70	60
NaOH (mM)	25	25	25	25	25	25	25	25	25
HEPES (mM)	10	10	10	10	10	10	10	10	10

All solutions were adjusted to pH 7.0 with methanesulfonic acid.

lent cations, currents were recorded with equivalent concentrations of different divalent cations in the external solution, as listed in Table 1, section A (Figures 3B and 3C). When the solution contained 50 mM Ba^{2+}, there was a small outward current and a large inward current (Figures 3B and 3C, green), comparable to the results shown in Figure 3A. When Ba^{2+} was replaced with Ca^{2+}, the outward current was similar, but the inward current was smaller, suggesting that BSC1 channels are less permeable to Ca^{2+} than to Ba^{2+} (Figure 3B, red). Substitution of Mg^{2+} for Ba^{2+} resulted in a slight outward current and a negligible inward current (Figure 3B, blue), indicating that BSC1 channels are not significantly permeable to Mg^{2+}. Substitution of either Co^{2+} (Figure 3C, red) or Cd^{2+} (Figure 3C, blue) resulted in essentially no outward or inward current, suggesting that both Co^{2+} and Cd^{2+} block BSC1 channels, similar to their effects on voltage-gated Ca^{2+} channels (Hille, 2001).

To determine the relative permeability of the BSC1 channel to different cations, the channels were activated by 15 ms depolarizations to 80 mV followed by repolarization to voltages ranging from −100 mV to 80 mV in recording solutions with different ionic compositions. The tail currents during the repolarizations were normalized to the maximum tail current at −100 mV and plotted against the repolarization voltage (Figure 3D). The reversal potentials were approximately 50 mV for Ba^{2+} and −10 mV for Na^+ and K^+. The relative permeabilities for Ba^{2+}, Na^+, and K^+ were then calculated using the extended constant-field equation as described in Experimental Procedures (Jan and Jan, 1976). The permeability ratios were $P_{Ba}/P_K \approx 30$ and $P_{Ba}/P_{Na} \approx 22$, indicating that Ba^{2+} is significantly more permeant through BSC1 channels than either Na^+ or K^+.

Since BSC1 channels can permeate Na^+ in the absence of Ca^{2+}, we examined the voltage dependence of channel gating when the external solution contained 50 mM Na^+ instead of 50 mM Ba^{2+} (Figure 1F). The voltage dependence of activation was shifted about 47 mV in the negative direction compared to Ba^{2+}, with an apparent gating charge of 1.3 ± 0.3 and a half-maximal activation voltage of 3 ± 7 mV. This shift is most likely the result of surface charges that are no longer being screened by the high concentration of Ba^{2+} ions. Therefore, BSC1 channels are activated at more physiological potentials when the external solution does not contain a high concentration of divalent cations.

BSC1 Channels Demonstrate an Anomalous Mole Fraction Effect

A characteristic property of voltage-gated Ca^{2+} channels is that they demonstrate permeabilities to different ions that depend on the concentrations of the ions in the bathing solution (Hille, 2001). For example, the current through a voltage-gated Ca^{2+} channel can be quite large if the solution contains only divalent (Ca^{2+} or Ba^{2+}) or monovalent (Na^+) ions. However, addition of a low concentration of Ca^{2+} or Ba^{2+} to a high concentration of Na^+ will decrease the current, because the divalent cations block the channel. This property results from the fact that Ca^{2+} channels can contain more than one ion in the pore, and it is called the anomalous mole fraction effect (Almers and McCleskey, 1984). Since the BSC1 channel is more permeable to Ba^{2+} than to Na^+, it was possible that this channel might also demonstrate the anomalous mole fraction effect. To test this hypothesis, currents were recorded using an external solution containing a constant concentration of 25 mM Na^+ and a concentration of free Ca^{2+} that varied from 2×10^{-6} to 20 mM (Table 1, section B). The free Ca^{2+} concentration was maintained by the addition of the Ca^{2+} chelators HEDTA or HIDA, as described by Almers et al. (1984). Ca^{2+} concentrations were used rather than activities following the procedures of Almers et al. (1984), because conversion to activities has been shown to be of questionable value in biology (Tsien, 1983). The peak currents were normalized to the maximal peak current in very low free Ca^{2+} (2×10^{-6} mM) and plotted against the concentration of free Ca^{2+} (Figure 4, circles). As can be seen, the current was large when there was very little free Ca^{2+} in the solution. In contrast, approximately 80% of the current was blocked by 0.2 μM free Ca^{2+}. When the free Ca^{2+} concentration was increased up to 20 mM, the current increased slightly, indicating that Ca^{2+} was permeating through the channel. These results suggest that low concentrations of Ca^{2+} prevented permeation by monovalent Na^+ through the BSC1 channels, whereas higher concentrations of Ca^{2+} resulted in Ca^{2+} currents.

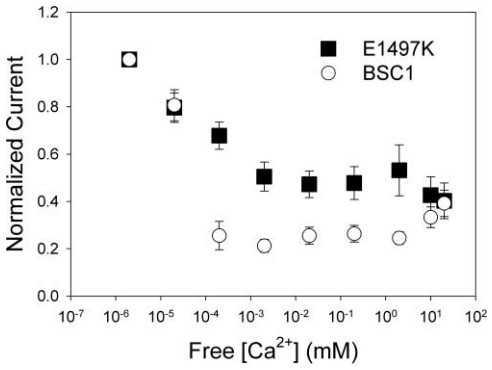

Figure 4. BSC1 Channels Demonstrate an Anomalous Mole Fraction Effect

Currents were recorded from oocytes injected with either 5 ng wild-type BSC1 RNA or 20 ng E1497K mutant RNA using an external solution containing increasing concentrations of free Ca^{2+}. The solution contained 25 mM Na^+, 10 mM HEPES, and 10 mM $Ca(OH)_2$ chelated with different amounts of HEDTA or HIDA to obtain free Ca^{2+} concentrations as follows: 2 nM, 20 nM, 200 nM, 2 μM, 20 μM, 200 μM, 2 mM, 10 mM, and 20 mM, following the procedures of Almers et al. (1984). Different amounts of TEAOH were used to adjust the pH and osmolarity of the solutions and to block the endogenous potassium channels. The stimulus protocol consisted of a single 15 ms depolarization from −100 mV to 80 mV followed by a repolarization to −100 mV. The tail current following each depolarization was normalized to the maximal tail current in the absence of external free Ca^{2+} and plotted against the free Ca^{2+} concentration. The results are shown for wild-type BSC1 (circles) and E1497K (squares). The symbols represent the means, and the error bars indicate standard errors of the mean.

Substitution of K for E1497 in the Pore Region of Domain III Reduced the BSC1 Channel Selectivity for Ba^{2+}

Selectivity in voltage-gated Na^+ and Ca^{2+} channels is strongly influenced by a ring of amino acids in the pore regions of the two types of channels (Chiamvimonvat et al., 1996; Favre et al., 1996). Voltage-gated Na^+ channels contain amino acids D, E, K, and A in the pore positions of domains I, II, III, and IV, respectively, whereas voltage-gated Ca^{2+} channels contain acidic residues (E) at the four positions. We compared the sequence of BSC1 with voltage-gated Na^+ and Ca^{2+} channels to determine if differences at these positions could be responsible for the Ca^{2+} selectivity of BSC1 (Table 2). The names of the channels that have been shown to function as voltage-gated Na^+ channels are shown in blue. These include all of the voltage-gated Na^+ channels from rat ($rNa_v1.1$–$rNa_v1.9$) and voltage-gated Na^+ channels from three insects, German cockroach *Blattella germanica* ($BgNa_v1$), *Drosophila melanogaster* ($DmNa_v1$), and housefly *Musca domestica* ($MdNa_v1$). Five insect voltage-gated Ca^{2+} channels are shown in red. The channels shown in green, including BSC1, have not previously been shown to encode functional voltage-gated ion channels.

All of the functional voltage-gated Na^+ channels have the signature sequence DEKA in the four domains, whereas all of the functional voltage-gated Ca^{2+} channels have the signature sequence EEEE. In contrast, BSC1 has the sequence DEEA, identical to that of Na^+ channels except in domain III. Substituting E for K in the domain III pore position of the rat $Na_v1.2$ Na^+ channel results in a channel that is more selective for Ca^{2+} than for Na^+ (Heinemann et al., 1992). Conversely, substituting K for E in the comparable position of the L-type Ca^{2+} channel results in a channel that is selective for monovalent cations (Yang et al., 1993). These results suggest that the E residue in domain III might be important for the Ca^{2+} selectivity of the BSC1 channel. To test this hypothesis, we substituted a K for E1497 in domain III of BSC1.

Currents through the E1497K mutant channel are shown in Figure 5A. When the external solution contained 50 mM Ba^{2+}, there was an outward current during the depolarization to 80 mV and a small inward tail current when the oocyte was repolarized to −100 mV (green). The outward current is most likely carried by K^+ ions, and the tail current is carried by Ba^{2+} ions. The inward Ba^{2+} current is significantly smaller than was seen for the wild-type BSC1 channel (compare Figure 5A, green, to Figure 3A, green), demonstrating that the E to K substitution decreased the permeability to Ba^{2+}. When the Ba^{2+} was replaced with 50 mM Ca^{2+}, the outward and inward currents were comparable (Figure 5A, red). When the Ba^{2+} was replaced with 50 mM Na^+, the outward current was larger, and the inward current was much larger (Figure 5A, blue). The larger inward current carried by Na^+ demonstrates that the mutant channel has greater permeability for Na^+ than for Ba^{2+}.

The relative permeabilities of the E1497K mutant channel to Na^+ (blue circles) and Ba^{2+} (green squares) were quantified by plotting the tail currents at different voltages following a 15 ms depolarization to 80 mV (Figure 5B), as described earlier for the wild-type channel. The reversal potentials were approximately −10 mV for Na^+ and −20 mV for Ba^{2+}. Using these values and the equation described earlier, the E1497K mutant channel has a selectivity ratio of $P_{Ba}/P_{Na} \approx 0.24$. Therefore, replacement of E1497 with a positively charged lysine made the BSC1 channel more permeable to Na^+ than to Ba^{2+}.

Since the E1497K mutation decreased the selectivity of the BSC1 channel for Ba^{2+}, it seemed likely that it would also eliminate the anomalous mole fraction effect. To test this hypothesis, currents were recorded with an extracellular solution that contained a constant concentration of 25 mM Na^+ with an increasing concentration of free Ca^{2+}. The peak currents were normalized to the maximal peak current in very low free Ca^{2+} (2×10^{-6} mM) and plotted against the concentration of free Ca^{2+} (Figure 4, squares). As for the wild-type BSC1 channel, the current was maximal in very low Ca^{2+}. However, the current decreased more gradually than was observed for the wild-type channel, and there was no increase in current at the highest Ca^{2+} concentrations. The decreasing current indicates that Ca^{2+} still blocks the E1497K channel and prevents conductance by Na^+, but the block requires higher concentrations of free Ca^{2+} than for the wild-type channel. The lack of current increase at the highest Ca^{2+} concentrations suggests that Ca^{2+} is less permeant through the E1497K mutant channel than the wild-type channel.

Phylogenetic Relationship of BSC1 to Voltage-Gated Na^+ and Ca^{2+} Channels

A phylogenetic tree was constructed to examine the relationship between BSC1 and other voltage-gated Na^+

Table 2. Sequence Comparison of BSC1 and Voltage-Gated Na^+ and Ca^{2+} Channels

Channel	Domain I	Domain II	Domain III	Domain IV
BSC1	QLITLDYWENVYN	RILCGEWTEPLWD	QVATFEGWMEVMA	RLMTSAGWNDVLG
DSC1	QLITLDYWENVYN	RILCGEWIEPLWD	QVATFEGWNEVMA	QLMTSAGWNDVLE
$CcNa_v1$	QVCTLDYWESVYN	RILCGKWIEPQWD	QTATLEGWFEVMQ	RISTAAGWNGVLE
$PpNa_v1$	QVCTLDYWESVFN	RILCGKWIEPQWD	QTATLEGWFEAMA	RISTAAGWNGVLD
$ApNa_v1$	QLVTLDYWENVYN	RVLCGEWIEPLYD	QVATFEGWFEVMR	RLSTSAGWNDVLK
$LbNa_v1$	QLLTQDYWEDVYN	RILCGEWIEPMYD	QVATFEGWMEIMA	RLATSAGWNDILG
$LoNa_v1$	RLMTQDYWENLYQ	RVLCGEWIESMWD	QVATFKGWINIMS	QMSTSAGWDGVLA
$BgNa_v1$ (para)	RLMTQDYWENLYQ	RVLCGEWIESMWD	QVATFKGWIQIMN	QMSTSAGWDGVLD
$DmNa_v1$ (para)	RLMTQDFWEDLYQ	RVLCGEWIESMWD	QVATFKGWIQIMN	QMSTSAGWDGVLD
$MdNa_v1$	RLMTQDFWEDLYQ	RVLCGEWIESMWT	QVATFKGWIQIMN	QMSTSAGWDGVLD
$rNa_v1.1$	RLMTQDFWENLYQ	RVLCGEWIETMWD	QVATFKGWMDIMY	QITTSAGWDGLLA
$rNa_v1.2$	RLMTQDFWENLYQ	RVLCGEWIETMWD	QVATFKGWMDIMY	QITTSAGWDGLLA
$rNa_v1.3$	RLMTQDYWENLYQ	RVLCGEWIETMWD	QVATFKGWMDIMY	QITTSAGWDGLLA
$rNa_v1.4$	RLMTQDYWENLFQ	RILCGEWIETMWD	QVATFKGWMDIMY	EITTSAGWDGLLN
$rNa_v1.5$	RLMQHDCWERLYQ	RILCGEWIETMWD	QVATFKGWMDIMY	QITTSAGWDGLLS
$rNa_v1.6$	RLMTQDYWENLYQ	RVLCGEWIETMWD	QVATFKGWMDIMY	QITTSAGWDGLLL
$rNa_v1.7$	RLMTQDYWENLYQ	RVLCGEWIETMWD	QVATFKGWMDIMY	QITTSAGWDGLLA
$rNa_v1.8$	RLMTQDSWERLYQ	RILCGEWIENMWV	QVATFKGWMDIMY	QITTSAGWDGLLS
$rNa_v1.9$	RVMTQDSWERLYR	RILCGEWIENMWG	QVATYKGWLEIMN	QITTSAGWDTLLN
rNa_x	RLMTQDYPELLYH	RILCGEWIENLWE	QVATYNGWISIMN	QVTTFSGWDTMLD
$DmCa_vA1$	QCVTLEGWTDVLY	QIMTGEDWNAVMY	TVSTFEGWPGLLY	RSATGEAWQEIMM
$MdCa_v1$	QCITLEGWTDVLY	QILTGEDWNVVMY	TVSTFEGWPTLLY	RSATGEAWQEIMM
$CcCa_v1$	QCTTLEGWTDVLY	QILTGEDWNAVMY	VVMTFEGWPSILE	RSATGENWQQIMM
$LbCa_v1$	QCVTMEGWTQVLY	QILTGEDWNEVMY	TVTTGEGWPMVLK	RCATGESWQQIML
$DmCa_vD1$	QCITMEGWTAILY	QILTGEDWNEVMY	AVQTGEGWPQVLQ	RCATGEAWPNIML

and Ca^{2+} channels (Figure 6). The channels that have been shown to function as voltage-gated Na^+ channels are shown in blue, and those that function as voltage-gated Ca^{2+} channels are shown in red. All of the mammalian voltage-gated Na^+ channels are located on a single branch of the tree. Similarly, all of the voltage-gated Ca^{2+} channels are located on a single branch of the tree. BSC1 is located on a unique branch, with its closest neighbor being DSC1, the *Drosophila* ortholog of BSC1. The DSC1 channel has never been functionally expressed. However, it has the same DEEA sequence as BSC1 (Table 2), and its close relationship suggests that it may also encode a Ca^{2+}-selective channel. Both of these proteins are as closely related to Ca^{2+} channels as they are to Na^+ channels, indicating that they may be descended from an ancestral channel that is intermediate between the voltage-gated Na^+ and Ca^{2+} channels.

The proteins that have not been shown to function as voltage-gated Na^+ channels are shown in green. All but two of these ($LoNa_v1$ and rNa_x) are located on unique branches of the tree. The sequences for those proteins also contain E in domain III comparable to BSC1, and therefore, they may also encode channels that are more selective for Ca^{2+}. Of the two exceptions, $LoNa_v1$ contains K in domain III and is on a branch with three genes that have been shown to encode voltage-gated Na^+ channels ($BgNa_v1$, $DmNa_v1$, and $MdNa_v1$) so that it may encode a true voltage-gated Na^+ channel. The other exception is rNa_x, which contains N in domain III and is on the branch with the other mammalian channels. This protein does not represent a voltage-gated Na^+ channel and most likely functions to sense Na^+ levels (Hiyama et al., 2002; Watanabe et al., 2003).

Discussion

We have demonstrated that *BSC1*, a gene originally identified because of its sequence similarity to voltage-gated Na^+ channels, encodes a functional voltage-gated cation channel when expressed in *Xenopus* oocytes. However, the properties of the BSC1 channel differ significantly from voltage-gated Na^+ channels in a number of ways. First, the channels are more selective for Ba^{2+} than for Na^+. Second, the kinetics of activation and inactivation are significantly slower than the kinetics of Na^+ channel gating. Third, the channel deactivates very slowly with a substantial tail current. Finally, Na^+ currents through the channel can be blocked by low concentrations of Ca^{2+}, resulting in an anomalous mole fraction effect. All of these properties are more similar to voltage-gated Ca^{2+} channels than to voltage-gated Na^+ channels.

Numerous previous attempts to obtain functional expression of several putative Na^+ channel proteins similar to BSC1, such as $CcNa_v1$ and DSC1, have failed (Nagahora et al., 2000; White et al., 1998). These channels possess the same DEEA signature in the putative pore region as BSC1, and they are phylogenetically related to BSC1 (Table 2 and Figure 6). Our data suggest that the failures may reflect the fact that BSC1 is a unique cation channel that is more permeable to Ca^{2+} and Ba^{2+} than to Na^+ and K^+. The unique ion selectivity and gating properties of the BSC1 channel clearly distinguish it from voltage-gated Na^+ channels, despite its extensive homology to known voltage-gated Na^+ channels.

The BSC1 channel exhibits markedly slower activation and inactivation compared to that of known Na^+ channels. The linker sequence connecting domains III and IV is highly conserved among functional Na^+ channels

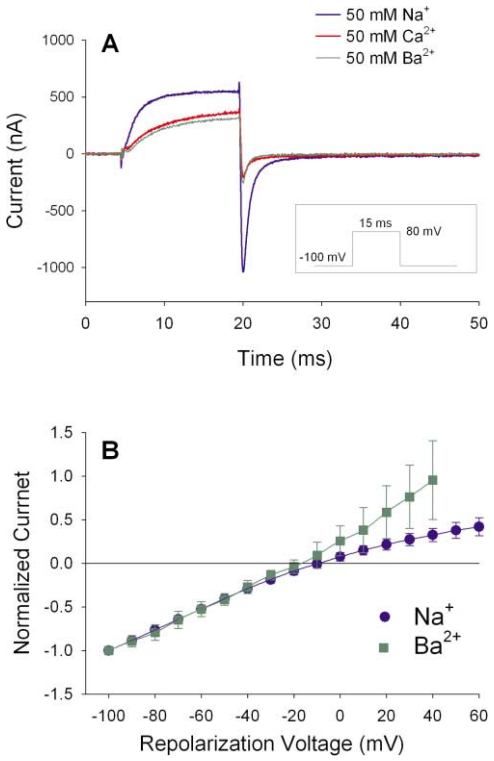

Figure 5. Substitution of E1497 with K Reduces the Selectivity for Ca^{2+}

(A) Currents were recorded from an oocyte injected with 20 ng E1497K RNA using an external solution consisting of either 50 mM NaOH + 45 mM TEAOH + 10 mM HEPES + 10 mM HEDTA (blue), 50 mM $Ca(OH)_2$ + 55 mM TEAOH + 5 mM HEPES (red), or 50 mM $Ba(OH)_2$ + 55 mM TEAOH + 5 mM HEPES (green). The protocol consisted of a depolarization from −100 mV to 80 mV for 15 ms followed by repolarization to −100 mV.

(B) Tail currents were measured by depolarization to 80 mV followed by repolarization to different potentials in each external solution, after which the tail currents were normalized to the maximal tail current and plotted against the repolarization voltage. The recording solutions were as follows: 50 mM Ba^{2+} (green squares) or 50 mM Na^+ (blue circles).

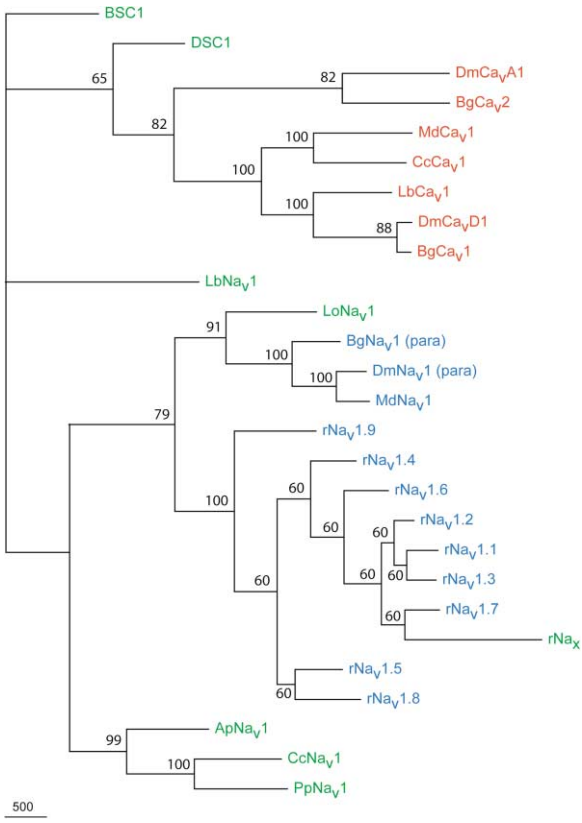

Figure 6. Phylogenetic Tree of BSC1 and Voltage-Gated Na^+ and Ca^{2+} Channels

A phylogenetic tree showing the relationship between BSC1 and voltage-gated Na^+ and Ca^{2+} channel α subunits was generated. This unrooted tree represents the optimal tree based on parsimony analysis of nucleotide sequences. To perform the analysis, the amino acid sequences were aligned using Clustal W (Thompson et al., 1994). The amino acid sequences in the alignments were then replaced with the published nucleotide sequences, and the nucleotide sequence alignments were subjected to analysis using the program PAUP* (Swofford, 1998). Divergent portions, including most of the terminal regions and the cytoplasmic loops between domains I-II and II-III, were excluded from the PAUP* analysis. The numbers at the nodes indicate the bootstrap values for 100 replications. When a number is not indicated, the bootstrap value was less than 50. Scale bar, 500 substitutions. The Ca^{2+} channel α1 subunit sequences are as follows: $BgCa_v1$ (*Blattella germanica*, German cockroach, GenBank accession number D31719), $BgCa_v2$ (*Blattella germanica*, GenBank accession number D31718), $CcCa_v1$ (*Cyanea capillata*, Scyphozoan jellyfish [Jeziorski et al., 1998]), $DmCa_vA1$ (*Drosophila melanogaster*, [Eberl et al., 1998]), $DmCa_vD1$ (*Drosophila melanogaster*, [Smith et al., 1996]), $LbCa_v1$ (*Loligo bleekeri*, squid [Kimura et al., 1997]), $MdCa_v1$ (*Musca domestica*, house fly [Grabner et al., 1994]). The invertebrate Na^+ channel and Na^+ channel-related sequences are from the following species: $ApNa_v1$ (*Aiptasia pallida*, sea anemone), $BgNa_v1$ (*Blattella germanica*, para^{CSMA}), BSC1 (*Blattella germanica*), $CcNa_v1$ (*Cyanea capillata*, CYNA1), $DmNa_v1$ (*Drosophila melanogaster*, para), DSC1 (*Drosophila melanogaster*), $LbNa_v1$ (*Loligo bleekeri*, squid Na channel), $LoNa_v1$ (*Loligo opalescens*, GFLN1), $MdNa_v1$ (*Musca domestica*, Msc Vssc1), and $PpNa_v1$ (*Polyorchis penicillatus*, Hydrozoan jellyfish, PpSCN1). The mammalian Na^+ channel sequences are all from *Rattus norvegicus*. References for all of the sodium channel sequences are listed in Goldin (2002).

and is involved in fast inactivation (Patton et al., 1992; West et al., 1992). This linker region is less conserved in the BSC1 protein, with the critical IFM motif being replaced by MFL (Liu et al., 2001). It is possible that this sequence variation is responsible for the slow inactivation of the BSC1 channel, although the F residue that is most important for fast inactivation is still present in BSC1.

The BSC1 channel demonstrates selectivity characteristics that are distinct from both voltage-gated Na^+ and Ca^{2+} channels. The Ba^{2+} to Na^+ permeability ratio (P_{Ba}/P_{Na}) for BSC1 is approximately 22. That is much lower than the permeability ratio for L-type Ca^{2+} channels ($P_{Ba}/P_{Na} \approx 470$ and $P_{Ca}/P_{Na} \approx 1170$) and much higher than the ratio for Na^+ channels ($P_{Ca}/P_{Na} \approx 0.1$) (Hille, 2001). These results indicate that the BSC1 channel has selectivity characteristics that are intermediate between those of Na^+ and Ca^{2+} channels. The mutation that replaces the negative charge in the pore region of domain III with a positive charge (E1497K) increased the selectivity of BSC1 for Na^+ ($P_{Ba}/P_{Na} = 0.24$) so that the mutant

channel is more similar to voltage-gated Na^+ channels. The E1497K mutation also decreased the inward rectification that was observed for wild-type BSC1 (compare Figures 3 and 5), but it did not eliminate block of Na^+ conductance by low concentrations of Ca^{2+} (Figure 4). Therefore, the glutamate residue in the pore region of domain III is important for the selectivity and rectification properties of BSC1, but block by Ca^{2+} also depends on other amino acids that differ between BSC1 and voltage-gated Na^+ channels.

The importance of additional residues in selectivity of Na^+ and Ca^{2+} channels has also been shown by the characteristics of a bacterial ion channel, NaChBac. The NaChBac channel consists of a single six-transmembrane-spanning segment whose sequence is similar to that of voltage-gated Ca^{2+} channels. This channel has an E in the pore position (Ren et al., 2001), and because it consists of a single domain, the functional channel has the signature sequence EEEE. However, NaChBac is more selective for Na^+ than for Ca^{2+} ($P_{Ca}/P_{Na} \approx 0.15$), and substitution of nearby residues converts it into a channel that is more selective for Ca^{2+}. For example, $P_{Ca}/P_{Na} \approx 73$ when LESWAS was replaced with LEDWAD, where **E** is the signature residue (Yue et al., 2002).

It has been proposed that voltage-gated Na^+ and Ca^{2+} channels evolved from K^+ channels and that Na^+ channels evolved after the subunit duplications leading to the Ca^{2+} channels (Hille, 1989; Strong et al., 1993). Strong et al. (1993) suggested that the original duplication event resulted in a two-domain channel consisting of domains I/III and II/IV, each of which then duplicated to result in the first four-domain Ca^{2+} channel. The primordial Na^+ channel then evolved from the Ca^{2+} channels and subsequently evolved independently in vertebrates and invertebrates (Strong et al., 1993). In this context, NaChBac may represent a descendant of the single-domain Ca^{2+}-selective channel that evolved from the K^+ channels, since it has characteristics intermediate between those of voltage-gated Na^+ and Ca^{2+} channels (Ren et al., 2001). NaChBac is more closely related in sequence to BSC1 and DSC1 than to voltage-gated Na^+ channels (data not shown), suggesting that BSC1 and related channels might represent the descendants of the primordial four-domain channels.

The two Na^+ channel genes identified in *Drosophila*, *DSC1* and *para* ($DmNa_v1$), are orthologs of *BSC1* and *para*^{CSMA} ($BgNa_v1$) from *Blattella germanica*. The *para* gene was identified based on temperature-sensitive paralysis phenotypes displayed by mutant alleles (Loughney et al., 1989). Consistent with these phenotypic effects, heterologous expression studies have demonstrated that para is a true voltage-gated Na^+ channel with biophysical and pharmacological properties similar to mammalian voltage-gated Na^+ channels (Warmke et al., 1997). In contrast, *DSC1* was identified based on sequence homology to an eel voltage-gated Na^+ channel (Salkoff et al., 1987), but it has never been functionally expressed in any heterologous systems. A mutation in the *DSC1* gene has been constructed using a P element insertion, and the mutant flies demonstrated impaired olfactory behavior, indicating that the DSC1 channel is involved in the processing of olfactory information (Kulkarni et al., 2002).

Our results show that BSC1 is a cation channel that might pass either Na^+ or Ca^{2+}, depending on the Ca^{2+} concentration, suggesting that BSC1 and para may play complementary roles in vivo. No native currents identical to those we recorded from BSC1 channels have been reported. It is possible that the functional characteristics of BSC1 are altered by association with accessory subunits, although no such subunits have yet been identified. Ca^{2+}-dependent plateau action potentials have been recorded in dorsal paired median neurons from the terminal abdominal ganglion of the cockroach *Periplaneta americana* (Amat et al., 1998). This slow depolarization was suggested to reflect a high-voltage activated Ca^{2+} current initiated by fast Na^+-dependent spikes (Amat et al., 1998). An intriguing possibility is that $BgNa_v1$ and BSC1 may be the two channels behind the fast initial depolarization and the plateau, respectively.

DSC1 and para demonstrate different patterns of expression in *Drosophila*. Based on in situ hybridization studies, para is the predominant Na^+ channel in *Drosophila*, being expressed ubiquitously throughout the CNS and PNS at all developmental stages (Hong and Ganetzky, 1994). In contrast, there are very few cells in either the CNS or PNS expressing DSC1 during embryonic and larval stages (Hong and Ganetzky, 1994). In pupal and adult stages, DSC1 and para have overlapping expression patterns in the CNS but distinct expression patterns in the PNS (Hong and Ganetzky, 1994). Based on immunolocalization studies of protein, DSC1 was observed only in neurons, with the highest density in synaptic regions and in axonal processes, but not in the cortical cell bodies in which para is highly expressed (Castella et al., 2001). These results further suggest that DSC1 and para serve different functions in the nervous system.

Tissue distribution of the BSC1 transcript also differs from that of para^{CSMA} ($BgNa_v1$). The para^{CSMA} transcript is most abundantly expressed in nerve, although it can also be detected in muscle (Liu et al., 2001). In contrast, the *BSC1* transcript is most abundantly expressed in muscle, but it is also broadly distributed in nerve cord, gut, and ovary (Liu et al., 2001). Furthermore, different tissues express different alternatively spliced variants of *BSC1*, including truncated variants containing only the first two of the four domains, which have been detected only in muscle (Liu et al., 2001). The broad tissue distribution of BSC1 and tissue-specific expression of alternatively spliced variants suggest that BSC1 channels may carry out distinct functions in different tissues (Liu et al., 2001).

In conclusion, our data demonstrate that BSC1 is a voltage-gated cation channel that is related to voltage-gated Na^+ channels but has many of the properties of voltage-gated Ca^{2+} channels. Channels that may be comparable are present in other invertebrate species, although none have yet been identified in vertebrates. Therefore, BSC1 appears to be the first functionally identified member of a novel family of voltage-gated cation channels with a close structural and evolutionary relationship to voltage-gated Na^+ and Ca^{2+} channels.

Experimental Procedures

Cloning Full-Length *BSC1* cDNA

To isolate the full-length *BSC1* cDNA, the entire coding region was amplified using two primers based on the 5′ and 3′ end sequences (Liu et al., 2001). A Kozak consensus sequence (GCCACCATGG)

was added around the ATG codon to increase the efficiency of translation. The BamH1 restriction recognition sequence was added to both primers to facilitate subsequent cloning. The entire coding region (6.9 kb) was amplified by polymerase chain reaction (PCR) using the Elongase Enzyme Mix (GIBCO/BRL, Rockville, MD). The amplified cDNA was then cloned into the pGH19 expression vector (kindly provided by Dr. B. Ganetzky, University of Wisconsin, Madison). A *BSC1* clone named ZL1 was sequenced to confirm that there were no mutations. This sequence represents a naturally occurring neuronal splice variant (Liu et al., 2001).

Site-Directed Mutagenesis

To replace E1497 with K in the pore-forming region of domain III, a 2.3 kb NsiI fragment encoding IIIS5 to the C terminus was subcloned from ZL1 into the pAlter-Ex1 vector (Promega Corp., Madison, WI). Site-directed mutagenesis was performed using the Altered Sites II in vitro Mutagenesis System (Promega Corp., Madison, WI) following the manufacturer's instructions. After the E1497K mutation was confirmed by DNA sequencing, the mutated NsiI fragment was excised from pAlter-Ex1 and cloned back into the ZL1 to produce the mutant *BSC1* clone.

Expression of the BSC1 Channel in *Xenopus* Oocytes

Stage V oocytes were removed from adult female *Xenopus laevis* frogs and prepared as previously described (Goldin, 1991). Oocytes were incubated in ND-96 media, which consists of 96 mM NaCl, 2 mM KCl, 1.8 mM $CaCl_2$, 1 mM $MgCl_2$, and 5 mM HEPES (pH 7.5), supplemented with 0.1 mg/ml gentamicin, 0.55 mg/ml pyruvate, and 0.5 mM theophylline. The ZL1 plasmid containing the BSC1 cDNA was linearized with NotI, and capped, full-length transcripts were synthesized in vitro using T7 polymerase (mMESSAGE mMACHINE kit, Ambion, Austin, TX). RNA was dissolved in 1 mM Tris-HCl (pH 7.5), and 5–20 ng BSC1 RNA was injected into each oocyte. Oocytes were incubated in ND96 at 20°C for 3–5 days before recording.

Electrophysiological Analysis

Voltage clamping of *Xenopus* oocytes was performed using the DAGAN CA-1 high performance cut-open oocyte clamp (DAGAN Corp., Minneapolis, MN), Axon DigiData 1321A Interface, and pClamp 8.1 (Axon Instruments, Inc., Burlingame, CA). Oocytes were perforated in the center of the vegetal pole and mounted on the voltage clamp stage fitted with a perfusion cannula connected to a syringe pump filled with internal solution. Agarose bridges coupling the headstage to the bath were filled with 0.5% low melting point agarose in 1 M NaCl (pH 7.5) and were fitted with 100 μm platinum wires to improve frequency response. The headstage manifold wells were filled with 1 M NaCl. Temperature in these experiments was maintained at 20°C by a Peltier device coupled to a feedback controller (HCC-100A, DAGAN Corp., Minneapolis, MN). Voltage was monitored through a 0.2–0.5 MΩ microelectrode filled with 3 M KCl, which was inserted through the animal pole of the oocyte. All recordings were obtained after stable baseline and ionic current levels were achieved. Series resistance compensation and P/4 subtraction were used in all recordings. Filter bandwidth was adjusted to approximately one-fourth the sampling rate. The internal solution consisted of 44 mM K_2SO_4, 5 mM Na_2SO_4, 10 mM EGTA-CsOH, and 10 mM HEPES-CsOH (pH 7.5). The compositions of the external solutions are shown in Table 1, section A.

The voltage dependence of activation was analyzed using a step protocol in which oocytes were depolarized from a holding potential of −100 mV to a range of potentials from −50 mV to 140 mV in 10 mV increments, followed by a return to −100 mV. The peak tail currents during the repolarizations were normalized to the maximum peak tail current and plotted against voltage. Conductance was calculated by individually fitting each curve with a two-state Boltzmann equation, $G = 1/(1 + \exp[-0.03937 \times z \times (V - V_{1/2})])$, in which G is the conductance, z is the apparent gating charge, V is the potential of the given pulse, and $V_{1/2}$ is the potential for half-maximal activation.

The kinetics of BSC1 activation were determined using a step protocol in which oocytes were depolarized from −100 mV to 80 mV for 1–150 ms, with 1 ms increments up to 30 ms and 5 ms increments thereafter, followed by repolarization to −100 mV. The peak tail current during the repolarization was then plotted versus the time of depolarization. The kinetics of BSC1 inactivation were determined using a step protocol in which oocytes were depolarized from −100 mV to 80 mV for 5–150 ms with 5 ms increments, and from 50 to 500 ms with 50 ms increments, followed by repolarization to −100 mV.

Relative permeability of the BSC1 channel to different cations was determined by recording currents using external solutions that contained only a single permeant ion at a concentration of 50 mM and then determining the reversal potential for each set of recording conditions. The compositions of the different solutions are shown in Table 1, section A. Because Na^+ and Ba^{2+} have different valences, the Goldman-Hodgkin-Katz equation could not be used to calculate the permeability of the channel. Therefore, the relative permeability of the BSC1 channel to Na^+, K^+, and Ba^{2+} was calculated using a simplified version of the extended constant-field equation as described by Jan and Jan (1976):

$$E_{rev} = \frac{RT}{F} \ln \frac{-b + (b^2 - 4ac)^{1/2}}{2a}, \text{ in which}$$

$$a = [K^+]_i + \frac{P_{Na}}{P_K}[Na^+]_i + 4\frac{P_{Ba}}{P_K}[Ba^{2+}]_i$$

$$b = ([K^+]_i - [K^+]_o) + \frac{P_{Na}}{P_K}[Na^+]_i - [Na^+]_o$$

$$c = -[K^+]_o + \frac{P_{Na}}{P_K}[Na^+]_o - 4\frac{P_{Ba}}{P_K}[Ba^{2+}]_o$$

In this equation, E_{rev} is the reversal potential of the cell, P_X is the permeability to cation X, $[X]_o$ is the concentration of X in the outside solution, $[X]_i$ is the concentration of X in the inside solution, R is the gas constant, T is absolute temperature, and F is Faraday's constant. This equation has been simplified by the fact that other permeant ions are not present on either the outside or inside of the cell. The concentrations of the permeant ions were determined by the experimental conditions, with $[K^+]_i = 88$ mM, $[Na^+]_i = 10$ mM, $[Ba^{2+}]_i = 0$, and only one permeant ion at a concentration of 50 mM on the outside of the cell during each experiment. Simultaneous equations were numerically solved to calculate the permeability ratios using the program Mathematica, Version 4.2 (Wolfram Research, Champaign, IL).

Phylogenetic Analysis

The amino acid sequences for all of the channels listed in the legend to Figure 6 were aligned using Clustal W (Thompson et al., 1994), after which the amino acid sequences in the alignments were replaced with the published nucleotide sequences. The nucleotide sequence alignments were then subjected to analysis using the program PAUP* (Swofford, 1998). Divergent portions, including most of the terminal regions and the cytoplasmic loops between domains I-II and II-III, were excluded from the PAUP* analysis.

Acknowledgments

We thank Mike Cahalan for advice on recording Ca^{2+} currents through BSC1 channels; George Gutman for help with the phylogenetic analysis; Jay Spampanato, Annie Lee, A.J. Barela, and Hai Nguyen for helpful discussions; and Brian Tanaka for excellent technical assistance. This work was supported in part by NSF grants IBN9696092 (K.D.) and IBN9808156 (K.D.), NIH Grant NS26729 (A.L.G.), and the Michigan State University Rackham Endowment Fund (K.D.). W.Z. was supported by a fellowship from the American Heart Association.

Received: September 10, 2003
Revised: December 22, 2003
Accepted: February 3, 2004
Published: April 7, 2004

References

Almers, W., and McCleskey, E.W. (1984). Non-selective conductance in calcium channels of frog muscle: calcium selectivity in a single-file pore. J. Physiol. *353*, 585–608.

Almers, W., McCleskey, E.W., and Palade, P.T. (1984). A non-selective cation conductance in frog muscle membrane blocked by micromolar external calcium ions. J. Physiol. *353*, 565–583.

Amat, C., Lapied, B., French, A.S., and Hue, B. (1998). Na^+-dependent neuritic spikes initiate Ca^{2+}-dependent somatic plateau action potentials in insect dorsal paired median neurons. J. Neurophysiol. *80*, 2718–2726.

Anderson, P.A.V., and Greenberg, R.M. (2001). Phylogeny of ion channels: clues to structure and function. Comp. Biochem. Physiol. B Biochem. Mol. Biol. *129*, 17–28.

Castella, C., Amichot, M., Bergé, J.-B., and Pauron, D. (2001). DSC1 channels are expressed in both the central and the peripheral nervous system of adult *Drosophila melanogaster*. Invert. Neurosci. *4*, 85–94.

Catterall, W.A. (2000). From ionic currents to molecular mechanisms: the structure and function of voltage-gated sodium channels. Neuron *26*, 13–25.

Chiamvimonvat, N., Perez-Garcia, M.T., Tomaselli, G.F., and Marbán, E. (1996). Control of ion flux and selectivity by negatively charged residues in the outer mouth of rat sodium channels. J. Physiol. *491*, 51–59.

Dong, K. (1997). A single amino acid change in the para sodium channel protein is associated with knockdown-resistance (*kdr*) to pyrethroid insecticides in German cockroach. Insect Biochem. Mol. Biol. *27*, 93–100.

Eberl, D.F., Ren, D., Feng, G., Lorenz, L.J., Van Vactor, D., and Hall, L.M. (1998). Genetics and developmental characterization of *Dmca1D*, a calcium channel α_1 subunit gene in *Drosophila melanogaster*. Genetics *148*, 1159–1169.

Favre, I., Moczydlowski, E., and Schild, L. (1996). On the structural basis for ionic selectivity among Na^+, K^+, and Ca^{2+} in the voltage-gated sodium channel. Biophys. J. *71*, 3110–3125.

Feng, G., Deak, P., Chopra, M., and Hall, L.M. (1995). Cloning and functional analysis of TipE, a novel membrane protein that enhances Drosophila *para* sodium channel function. Cell *82*, 1001–1011.

Goldin, A.L. (1991). Expression of ion channels by injection of mRNA into *Xenopus* oocytes. Methods Cell Biol. *36*, 487–509.

Goldin, A.L. (2002). Evolution of voltage-gated Na^+ channels. J. Exp. Biol. *205*, 575–584.

Grabner, M., Bachmann, A., Rosenthal, F., Striessnig, J., Schulz, C., Tautz, D., and Glossmann, H. (1994). Insect calcium channels. Molecular cloning of an α_1-subunit from housefly (*Musca domestica*) muscle. FEBS Lett. *339*, 189–194.

Heinemann, S.H., Terlau, H., Stühmer, W., Imoto, K., and Numa, S. (1992). Calcium channel characteristics conferred on the sodium channel by single mutations. Nature *356*, 441–443.

Hille, B. (1987). Evolutionary origins of voltage-gated channels and synaptic transmission. In Synaptic Function, G.M. Edelman, W.E. Gall, and W.M. Cowan, eds. (New York: John Wiley & Sons), pp. 163–176.

Hille, B. (1988). Evolutionary origin of electrical excitability. In Cellular Mechanisms of Conditioning and Behavioral Plasticity, C.D. Woody, D.L. Alkon, and J. L. McGaugh, eds. (New York: Plenum Press), pp. 511–518.

Hille, B. (1989). Ionic channels: evolutionary origins and modern roles. Q. J. Exp. Physiol. *74*, 785–804.

Hille, B. (2001). Ion Channels of Excitable Membranes. (Sunderland, MA: Sinauer Associates, Inc.).

Hiyama, T.Y., Watanabe, E., Ono, K., Inenaga, K., Tamkun, M.M., Yoshida, S., and Noda, M. (2002). Na_x channel involved in CNS sodium-level sensing. Nat. Neurosci. *5*, 511–512.

Hong, C.-S., and Ganetzky, B. (1994). Spatial and temporal expression patterns of two sodium channel genes in *Drosophila*. J. Neurosci. *14*, 5160–5169.

Jan, L.Y., and Jan, Y.N. (1976). L-Glutamate as an excitatory transmitter at the *Drosophila* larval neuromuscular junction. J. Physiol. *262*, 215–236.

Jan, L.Y., and Jan, Y.N. (1992). Tracing the roots of ion channels. Cell *69*, 715–718.

Jeziorski, M.C., Greenberg, R.M., Clark, K.S., and Anderson, P.A.V. (1998). Cloning and functional expression of a voltage-gated calcium channel α_1 subunit from jellyfish. J. Biol. Chem. *273*, 22792–22799.

Kimura, T., Shouno, O., Hirota, K., Saito, T., Matsumoto, G., and Sato, C. (1997). Molecular cloning and characterization of a putative neural calcium channel α_1-subunit from squid optic lobe. Biochem. Biophys. Res. Commun. *230*, 147–154.

Kulkarni, N.H., Yamamoto, A.H., Robinson, K.O., Mackay, T.F.C., and Anholt, R.R. (2002). The DSC1 channel, encoded by the *smi60E* locus, contributes to odor-guided behavior in *Drosophila melanogaster*. Genetics *161*, 1507–1516.

Kuruma, A., and Hartzell, H.C. (2002). Dynamics of calcium regulation of chloride currents in *Xenopus* oocytes. Am. J. Physiol. *276*, C161–C175.

Liu, Z., Chung, I., and Dong, K. (2001). Alternative splicing of the *BSC1* gene generates tissue-specific isoforms in the German cockroach. Insect Biochem. Mol. Biol. *31*, 703–713.

Loughney, K., Kreber, R., and Ganetzky, B. (1989). Molecular analysis of the *para* locus, a sodium channel gene in Drosophila. Cell *58*, 1143–1154.

Nagahora, H., Okada, T., Yahagi, N., Chong, J.A., Mandel, G., and Okamura, Y. (2000). Diversity of voltage-gated sodium channels in the ascidian larval nervous system. Biochem. Biophys. Res. Commun. *275*, 558–564.

Patton, D.E., West, J.W., Catterall, W.A., and Goldin, A.L. (1992). Amino acid residues required for fast sodium channel inactivation. Charge neutralizations and deletions in the III-IV linker. Proc. Natl. Acad. Sci. USA *89*, 10905–10909.

Ren, D., Navarro, B., Xu, H., Yue, L., Shi, Q., and Clapham, D.E. (2001). A prokaryotic voltage-gated sodium channel. Science *294*, 2372–2375.

Salkoff, L., Butler, A., Wei, A., Scavarda, N., Giffen, K., Ifune, C., Goodman, R., and Mandel, G. (1987). Genomic organization and deduced amino acid sequence of a putative sodium channel gene in *Drosophila*. Science *237*, 744–748.

Smith, L.A., Wang, X., Peixoto, A.A., Neumann, E.K., Hall, L.M., and Hall, J.C. (1996). A *Drosophila* calcium channel α1 subunit gene maps to a genetic locus associated with behavioral and visual defects. J. Neurosci. *16*, 7868–7879.

Smith, T.J., Lee, S.H., Ingles, P.J., Knipple, D.C., and Soderlund, D.M. (1997). The L1014F point mutation in the house fly *Vssc1* sodium channel confers knockdown resistance to pyrethroids. Insect Biochem. Mol. Biol. *27*, 807–812.

Spafford, J.D., Spencer, A.N., and Gallin, W.J. (1999). Genomic organization of a voltage-gated Na^+ channel in a hydrozoan jellyfish: insights into the evolution of voltage-gated Na^+ channel genes. Receptors Channels *6*, 493–506.

Strong, M., Chandy, K.G., and Gutman, G.A. (1993). Molecular evolution of voltage-sensitive ion channel genes: on the origins of electrical excitability. Mol. Biol. Evol. *10*, 221–242.

Swofford, D.L. (1998). PAUP*: Phylogenetic Analysis Using Parsimony (*and Other Methods), Version 4. (Sunderland, MA: Sinauer Associates, Inc.).

Tan, J., Liu, Z., Nomura, Y., Goldin, A.L., and Dong, K. (2002a). Alternative splicing of an insect sodium channel gene generates pharmacologically distinct sodium channels. J. Neurosci. *22*, 5300–5309.

Tan, J., Liu, Z., Tsai, T.-D., Valles, S.M., Goldin, A.L., and Dong, K. (2002b). Novel sodium channel gene mutations in *Blattella germanica* reduce the sensitivity of expressed channels to deltamethrin. Insect Biochem. Mol. Biol. *32*, 445–454.

Thompson, J.D., Higgins, D.G., and Gibson, T.J. (1994). CLUSTAL W: improving the sensitivity of progressive multiple sequence alignment through sequence weighting, positions-specific gap penalties and weight matrix choice. Nucleic Acids Res. *22*, 4673–4680.

Tsien, R.Y. (1983). Intracellular measurements of ion activities. Annu. Rev. Biophys. Bioeng. *12*, 91–116.

Warmke, J.W., Reenan, R.A., Wang, P., Qian, S., Arena, J.P., Wang, J., Wunderler, D., Liu, K., Kaczorowski, G.J., Van der Ploeg, L.H., et

al. (1997). Functional expression of *Drosophila para* sodium channels. Modulation by the membrane protein *tipE* and toxin pharmacology. J. Gen. Physiol. *110*, 119–133.

Watanabe, U., Shimura, T., Sako, N., Kitagawa, J., Shingai, T., Watanabe, E., and Yamamoto, T. (2003). A comparison of voluntary salt-intake behavior in Na_x-gene deficient and wild-type mice with reference to peripheral taste inputs. Brain Res. *967*, 247–256.

West, J.W., Patton, D.E., Scheuer, T., Wang, Y., Goldin, A.L., and Catterall, W.A. (1992). A cluster of hydrophobic amino acid residues required for fast Na^+ channel inactivation. Proc. Natl. Acad. Sci. USA *89*, 10910–10914.

White, G.B., Pfahnl, A., Haddock, S., Lamers, G., Greenberg, R.M., and Anderson, P.A. (1998). Structure of a putative sodium channel from sea anemone *Aiptasia pallida*. Invert. Neurosci. *3*, 317–326.

Yang, J., Ellinor, P.T., Sather, W.A., Zhang, J.-F., and Tsien, R.W. (1993). Molecular determinants of Ca^{2+} selectivity and ion permeation in L-type Ca^{2+} channels. Nature *366*, 158–161.

Yue, L., Navarro, B., Ren, D., Ramos, A., and Clapham, D.E. (2002). The cation selectivity filter of the bacterial sodium channel, NaChBac. J. Gen. Physiol. *120*, 845–853.